Peer-reviewed version available at Crystals 2018, 8, 395; doi:10.3390/cryst8100395

Highly visible photoluminescence from Ta doped structures of ZnO films grown by HFCVD

V. Herrera [1], T. Díaz-Becerril [1,] *, E. Reyes-Cervantes[2], G. García-Salgado[1], R. Galeazzi[1], C. Morales[1], E. Rosendo[1], A. Coyopol[1], R. Romano[1], F.G. Nieto-Caballero[1]

[1] Centro de Investigación en Dispositivos Semiconductores, Universidad Autónoma de Puebla, 14 sur y Av. San Claudio, C.U., Edif. IC-5, San Manuel 72570, Puebla, México.
[2] Centro Universitario de Vinculación y Transferencia de Tecnología, Prol. de la 24 sur esq. con Av. San Claudio, C.U., Edif. CUVyTT, San Manuel 72570, Puebla, México.
* Correspondence: tomas.diaz.be@gmail.com; Tel.: +52-222-229-5500 ext. 7871

Abstract: Tantalum doped ZnO structures (ZnO:Ta) were synthesized and some of their characteristics were studied. ZnO material was deposited on silicon substrates by using a hot filament chemical vapor deposition (HFCVD) reactor. The raw materials were a pill made of a mixture of ZnO and Ta_2O_5 powders, and molecular hydrogen was used as a reactant gas. Percentage of tantalum was varied from 0 to 500mg by varying the percentage of tantalum oxide in the mixture of the pill source, by holding a fixed amount of 500mg of ZnO in all experiments.

X-ray diffractograms confirmed the presence of zinc oxide in the wurtzite phase and metallic zinc with a hexagonal structure, and no other phase was detected. Displacements to lower angles of reflection peaks, compared with those from samples without contamination, were interpreted as the inclusion of the Ta atoms in the matrix of the ZnO. This fact was confirmed by EDS and XRD measurements.

From SEM images from undoped samples exhibited mostly micro sized semi-spherical structures while doped samples displayed a trend to grown as nanocrystalline rods. The presence of tantalum during the synthesis affects the way of the growth.

Green photoluminescence at naked eye was observed when Ta doped samples were illuminated by ultraviolet radiation and confirmed by PL spectra. PL intensity on Ta doped ZnO varied from those undoped samples up to 8 times.

Keywords: Zinc oxide, tantalum oxide, ZnO:Ta doped films, substitutional alloy.

1. Introduction

In recent years, ZnO has become one of the most studied materials due to its very interesting properties in optoelectronic devices application such as; room temperature lasers [1], light emitting diodes [2,3], ultraviolet (UV) detectors [4], field-emission displays[5,6], photonic crystals [7], solar cells [8,9] and sensing in the nano-size range[10,11]. The control of its properties is critical in the context of novel applications. For this reason, a better understanding of the synthesis of microstructures/nanostructures with different morphologies is important and necessary to achieve objectives and applications on materials for the modern world. A profitable, simple and easily scalable method to synthesize the material is the hot filament chemical vapor deposition (HFCVD). This technique allows us the production of multifunctional structures to a larger scale. In addition, it is possible to have control of the material properties by only changing the synthesis conditions.

An important issue regarding applications in electronic and optoelectronic technologies is the doping. ZnO exhibit naturally n type conductivity because the presence of punctual defects such as zinc interstitial and/or oxygen vacancies in its matrix [12,13], and conductivity type p is not easy to

obtain due to the compensation effect that impedes this [3,12]. However, some other properties such as optical emission can be changed when ZnO is contaminated. It is reported light emission, in the UV-visible range, can be obtained when the material is doped with transition metals.

Also has been reported green emission around 510 nm when copper atoms are incorporated in ZnO films [14–16]. The luminescence was ascribed to the existence of oxygen vacancies. Other transition metals when are introduced to the ZnO such as Al, Li, Co, and Mn, also has been reported to exhibit emission in different ranges, however, the wavelength of emission and intensity depended on the process and technique of the growth [17–19]. Similarly, yellow emission has been observed when the ZnO synthesis is performed by chemical techniques. This emission was assigned to the existence of oxygen interstitials [20].

Ta is an atom that has been introduced in ZnO to change the properties of the material. It was found the T atoms can substitute Zn atoms in ZnO matrix modifying the electrical and optical properties of the films. Some uses include as photoactinic and TCO among others. However, information on changes on photoluminescent properties with the incorporation of Ta in ZnO material is missing.

To investigate on the effect of contamination of ZnO with Ta atoms, ZnO core-shell doped with tantalum structures were fabricated, and the optical and structural properties were studied, by comparison, undoped structures also were prepared to observe the effect of dopant.

The results shown, the morphology of structures is modified with the incorporation of tantalum in the process this effect increases the specific area of the material. The size of the core-shell structures is reduced as the Ta_2O_5% is incorporated into the growth process. The core-shell structures consist of a core composed of metallic zinc and a shell composed by ZnO nanocrystals become small as the Ta is increased to the process.

Because the temperature process is higher of the fusion point of the zinc metallic, atoms from the core diffuse through the intergrain frontiers of ZnO introducing a great number of zinc interstitials that seems as responsible for the greatly visible emission observed in the experiment. Luminescent emission is centered in 495nm and it can be observed to the naked eye. Recombination trough zinc interstitials oxygen vacancies in the volume of the ZnO grain has been invoked by other authors to explain the origin of the green emission. In this case that could be the origin of the increase in the intensity of the PL.

Ta seems no to introduce radiative centers that contribute to the PL. while the role of the Ta is to control the electric properties of the structures. Ta is a deep donor that contribute to reduce the resistivity of the ZnO grains, which corroborates the observed with other authors that studied similar structures, where show that tantalum is incorporated in the lattice of ZnO and act as a donor impurity.

2. Materials and Methods

Films obtained in this work were grown by HFCVD approach (High Filament Chemical Vapor Deposition), this reactor has a reaction chamber formed in the central section of a quartz tube, and this tube has at each end a metal caps of stainless steel, it is important to ensure an isolation of the inside of chamber reaction with the atmosphere, this because used gases inside the chamber are highly pyrophoric. Inside the quartz tube, the reaction chamber is formed by the following elements: a sprinkler, it is used to transport to the system a reactant gas, in all these experiments, hydrogen was used to grown us films, a filament of tungsten, that is used to elevate temperature inside the chamber (2000°C was used in this experiments), two supports, one used to place the source pill and the other one to place the substrate to obtain the films.

Each pill source was performed making a mixture of ZnO powder (Mallinckrodt Chemicals CAS 1314-13-2) with a powder of Ta_2O_5 (ALDRICH CAS 1314-61-0), in all the pellets fabricated, quantity of ZnO was the same of 500mg, whereas quantity of tantalum oxide was varied in a percentage of 0%, 10%, 20%, 40%, 50%, and 60% regarding to 500mg of ZnO, i.e. 500mg ZnO + 0gr Ta_2O_5, 500mg ZnO + 50mg Ta_2O_5, 500mg ZnO + 100mg Ta_2O_5, and so on. After of this, each mixture was scrambled until getting a homogenous powder, and next, each mix was pressed in a hydraulic press to 1 Ton in

a Making Pellets machine (CrushIR 181-1100), obtaining pills with a disk shape of 10mm in diameter and 5mm of height.

After a pill is collocated inside the reaction chamber, all these presented films were grown on silicon substrates with a temperature of 800°C in the substrate. Process is as follows: chamber is cleaned of substances in atmosphere, to do this, reactor is sealed and a flow of hydrogen is passed twice through the reactor, next the hydrogen flow is maintained inside the chamber until ¾ of capacity of the system, and now the temperature is turned on to 2000°C, this last process stands for 3 minutes.

At first, hydrogen inside the reaction chamber is in molecular form (H_2), but when temperature is elevated to 2000°C this gas is dissociated, in this phase, hydrogen is highly reagent, this fact makes that gas formed to attack the pill source forming a flow of gases inside the chamber, this flow is constituted by the precursors in the pill, i.e. ZnO and Ta_2O_5, however, some additionally reactions could occur with the gas and the substrate [21]. Finally, by the reactor dynamic, gases are transported to the substrate where the film is obtained, optical and structural properties of this were studied by X-ray, SEM, EDS; Hall Effect, and PL techniques.

The crystalline structure and orientation of the crystallites were studied using X-ray diffraction (BRUKER D8 with Cu Kα radiation (λ=1.541Å)), Raman spectra were taken with a RAM HR800 Raman spectrometer equipped with an Olympus BX41 microscope, a 632.8nm He-Ne laser was used as the excitation source. Surface morphology and composition of the films were examined with two systems, the low resolution was taken with a system SEM Jeol model 6610LV equipped with an INCA energy dispersive X-ray attached to this, and the high resolution was analyzed with a field emission scanning electron microscope FESEM JSM 5400LV equipped with a NORAN energy dispersive X-ray spectrometer. Profilometry and roughness analysis of the films was taken with a surface profiler Dektak 150. Photoluminescence measurements were performed at room temperature with a spectrofluorometer FluroMax 3, equipped with an emission detector with high sensibility and a 150W xenon lamp to excite the samples. Electrical properties of the films were determined with a system of Hall Effect from Ecopia Company model HMS-5000, using a magnetic field of 0.5T.

3. Results and Discussion

3.1. Structural characterization XRD

The diffractograms of films of polycrystalline zinc oxide doped with tantalum are shown in **Figure 1**, and a non-contaminated spectrum of ZnO is presented as a reference. For uncontaminated ZnO material (**Figure 1**a), the presence of diffraction peaks indicates the material possess a polycrystalline structure. Three well distinctive diffraction peaks placed at 2θ= 32°, 34.6°, 36.4°, corresponding to planes (100) (002) (101) are identified and matched with a hexagonal (wurtzite) ZnO crystalline structure (pdf card 075-0576). Additionally, some other diffractions peaks can be seen at 2θ= 47.8°, 56.8°, 63.1°, 68.0°and 69.3° corresponding to reflections on (102) (110) (103) (112) and (201) planes of wurtzite ZnO structure respectively. The presence of Zn phase was identified by the peaks placed at 2θ= 39.2°, 43.3° and 54.5° corresponding to planes (100), (101) and (102) of Zn in hexagonal phase (pdf card 004-0831).

The diffraction peaks from ZnO:Ta samples are presented in **Figure 1**(b-f). It can be seen some differences from that of reference sample (**Figure 1**a). As can be observed, the peak of ZnO in 2θ=69.3° is vanishing peaks in the other range, for that reason to get a better view of other peaks, we plotted the same diffraction patterns in a range from 2θ=30° to 66° in **Figure 2**. In this graphs, it is possible to observe an additional diffraction peak arising at 2θ= 66.98° corresponding to the structure of $ZnTa_2O_6$, suggesting some Ta atoms are incorporated into the ZnO lattice (pdf card 049-0746) [22]. Because the atomic radii of Ta (0.78 Å) are very similar to Zn atoms (0.82Å) these contaminants easily replace some zinc atoms in the ZnO network without making abrupt changes in the ZnO lattice. In us case, a small expansive stress in lattice of ZnO can be observed in 2θ=63.1, corresponding to the plane (103), this stress is causing that this peak shifts to lower angles (red arrows in **Figure 2**c, d), but no in all diffractions can be observed clearly this peak [23,24].

Preprints (www.preprints.org) | NOT PEER-REVIEWED | Posted: 27 July 2018 doi:10.20944/preprints201807.0535.v1

Peer-reviewed version available at Crystals 2018, 8, 395; doi:10.3390/cryst8100395

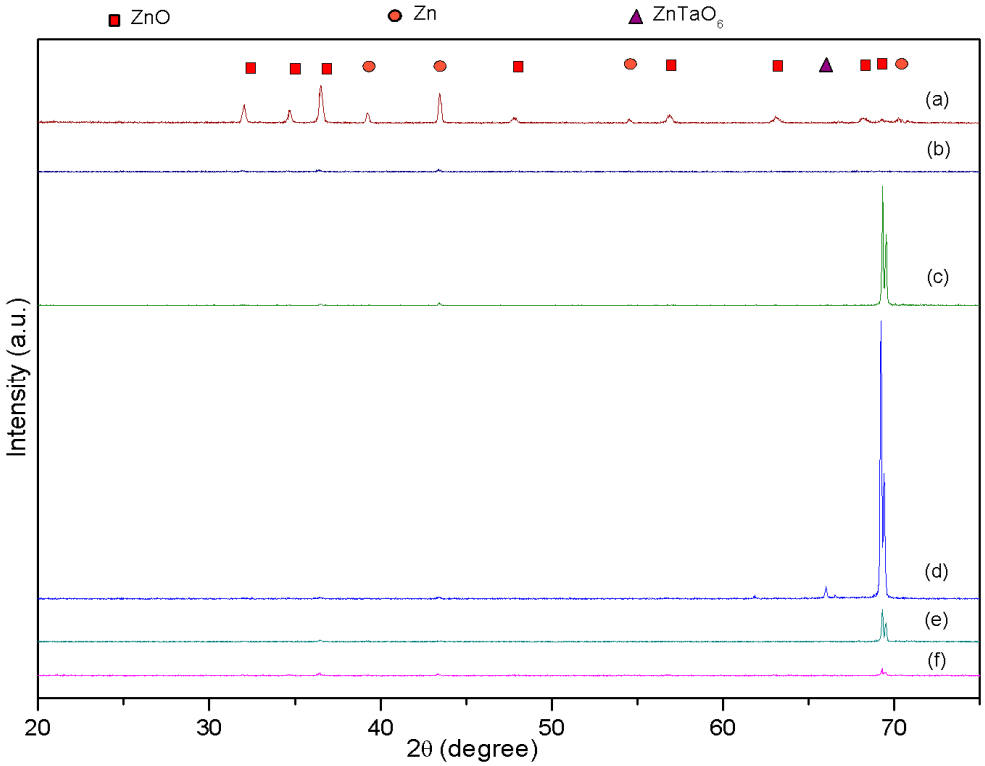

Figure 1.- XRD Patterns for (a) un-doped ZnO film, and ZnO:Ta doped films growned with a pellet of (b)10%, (c) 20%, (d) 40%, (e) 50% and (f) 60% of Ta_2O_5.

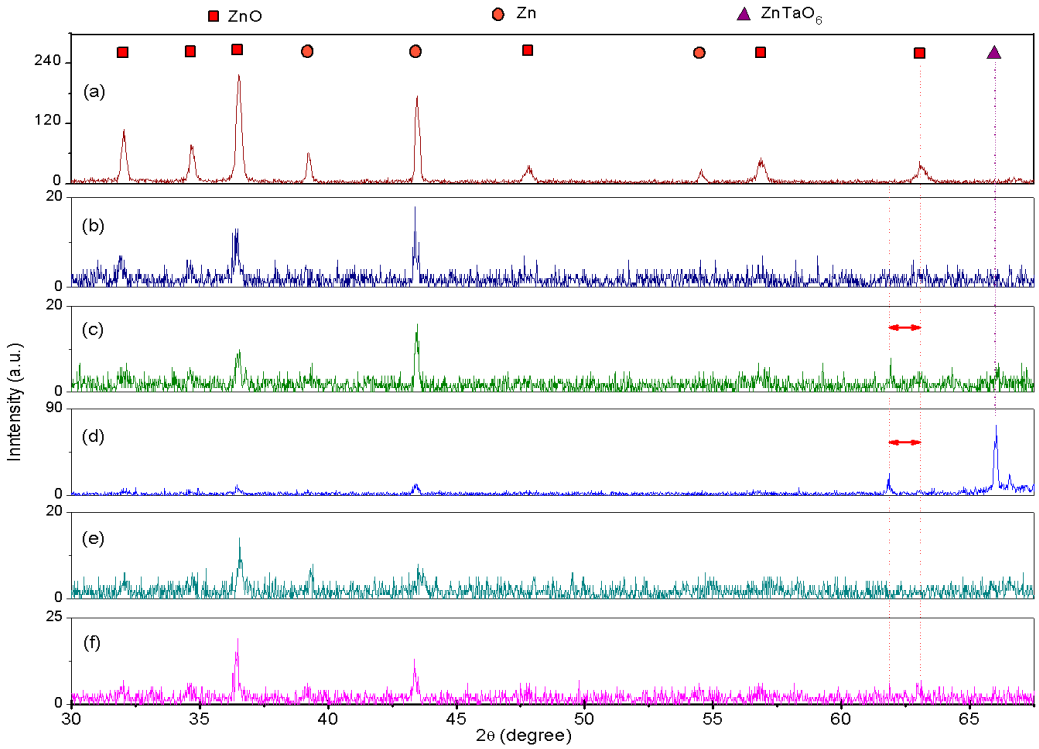

Figure 2.- Patterns for (a) un-doped ZnO film, and ZnO:Ta doled films growned with a pellet of (b)10%, (c) 20%, (d) 40%, (e) 50% and (f) 60% of Ta_2O_5 in a range from 2θ=30° to 66°.

It is interesting to note the principal peak of ZnO at 2θ = 36.4° in samples Ta contaminated and corresponding to (101) plane changes strongly in intensity as the concentration of Ta is increased in the process (**Figure 2**). This result suggests us that the high content of Ta may lead to the degradation

of ZnO crystallinity. The other ZnO peaks also become small and broad and it could be an indication that tantalum atoms in the HFCVD process could modify the crystalline orientation of the growth and from here modify the film morphology.

Diffraction peaks were analyzed with software HighScore Plus of PANalytical, every profile was approximated using a standard Caglioti function with a Pseudo-Voight profile fitting, results are shown in **Table 1**.

Table 1. Lattice parameters and crystallite size for ZnO and ZnO:Ta doped films obtained.

Reference name	d (Å)	(hkl)	a (Å)	c (Å)	Average crystallite size (nm)
ZnO	2.5869	(002)	3.2406	5.1738	224
ZnO50Ta	2.4653	(101)	3.2361	5.1841	155
ZnO100Ta	1.3542	(201)	3.2401	5.1806	142
ZnO200Ta	1.3561	(201)	3.2448	5.1831	134
ZnO250Ta	1.3546	(201)	3.2407	5.1874	129
ZnO300Ta	1.3551	(201)	3.2419	5.1895	122

Analyzing the diffraction chart, it can be see the three important diffraction peaks of (100), (002) and (101), planes of ZnO are diminished with the introduction of Ta in the ZnO process which it could mean the growth in that direction is inhibited while the growth along (201) is favored. According to data obtained and presented in **Table 1**, can be seen that crystallite size of ZnO is bigger than crystallites of ZnO:Ta doped, because when ZnO is doped with tantalum atoms crystallite size decrease strongly, and after of this crystallite size decrease slowly, in this case, this fact could be an indicative that tantalum atoms is creating this effect.

According to other reviewed reports, when ZnO is doped with tantalum, crystallite size is modified, but there is no a consensus of increment or decrement in crystallite size in ZnO:Ta doped films, this fact seems to be more affected by technique used to grow the film, even when ZnO is doped with other materials, crystallite size is increasing sometimes, and decreasing other ones [22,24,25]. For example, K. Bang et al reported the effect of lithium contamination in ZnO films, they found the (002) planes of ZnO was reduced as the Li content was increased that was interpreted as a degradation of the ZnO crystallinity while an increase in the grain size is observed as the concentration of lithium increased [26]. Also has been reported that the presence of metallic zinc is associated to the existence of core-shell structures where metallic zinc is the core and ZnO nanocrystals are composing the shell [21].

3.2. Raman mesuarements

The room temperature Raman spectra for undoped and Ta-doped ZnO in the range of 100 to 1000 cm^{-1} are presented in **Figure 3**. Three main bands are observed for pure ZnO (**Figure 3**a). A peak labeled E_2 (High) at 437 cm^{-1} is known as active optical phonon mode. Vibrational modes at 97 cm^{-1} known as E_2 (LO) and 570 cm^{-1} known as A_1 (LO) are also observable on the spectra. Presence of the three observed vibrations, in our measurements, confirms that the material synthesized have wurtzite hexagonal structure [27–30].

It was reported that a broad Raman band at about 570 cm^{-1} may be originate from defects related phonon mode, O-vacancies related stable complexes [31], zinc interstitials or from the disorder-activated B1(High) silent mode [32] of w-ZnO.

It is well known when metallic zinc particles are exposed to air or/and to an oxygen environment a $Zn_{1+x}O$ defective zinc oxide with Zn ion in interstitial position is formed around the metallic zinc [33] and a broad Raman band with a peak centered at 560 cm^{-1} is seen on the spectra. If it is assumed the Raman band centered at 563 cm^{-1}, on **Figure 3**a, has a contribution due to the formation of a

Preprints (www.preprints.org) | NOT PEER-REVIEWED | Posted: 27 July 2018 doi:10.20944/preprints201807.0535.v1

Peer-reviewed version available at Crystals 2018, 8, 395; doi:10.3390/cryst8100395

defective oxide then this result suggests us that our material is a core-shell type, where the core is metallic zinc and the shell is ZnO grains.

Moreover, the undoped and Ta-doped ZnO samples were grown under oxygen deficient environment and therefore the synthesized material contains a great number of oxygen vacancies and zinc interstitials [12,34,35] and they could also contribute to broadening of the Raman band observed at 563 cm^{-1}.

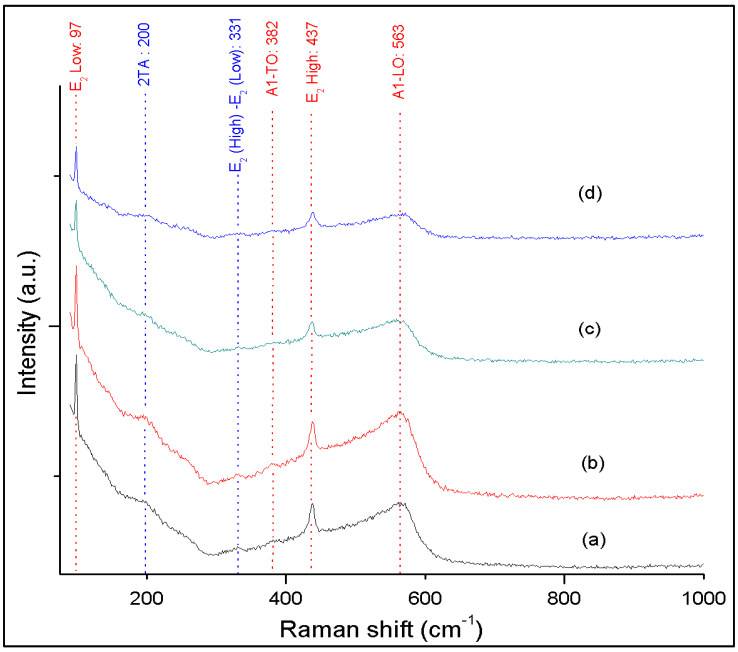

Figure 3. – Raman shift from samples (a) undoped, (b) 50mg, (c) 200mg, and (d) 300mg of Ta_2O_5.

Raman spectra from Ta doped ZnO are shown in **Figure 3**b-d. It can be seen that all the peaks found to correspond to that from the undoped sample (**Figure 3**a) the only difference is the reduction in the intensity of the E_2 (high) vibration and a broadening of both the second order and A_1 (LO) modes.

This observation could be an indication that Ta is encrusted in the ZnO matrix and induces small disorder in the lattice. The reduced intensity in the E_2 (high) peak might be related to the degradation on the crystalline quality observed by X-Ray diffraction we can expect those tantalum atoms when incorporated in the film induce change in the bonds strength between zinc and oxygen, therefore crystallinity is affected by this process, as have been observed in XRD results.

3.3. SEM and EDS estudies

Analysis SEM was carried out to observe the film morphology and they are presented in **Figure 4**. It can be seen the surface morphology changes as the percentage of Ta_2O_5 is increased in the pill source. Picture for undoped ZnO film (**Figure 4**a) shows a morphology with a high density of big sphere shapes and both density and size of this structures reduce or even disappear as the Ta_2O_5 content is increased in the process (**Figure 4**b-f). A magnification drawn on those samples (**Figure 5**) shows shape details of their morphology.

Micrographs taken on Ta doped ZnO samples (**Figure 4**b-f) show the roughness of the surface decreases as the content of Ta_2O_5 is increased in the pill source, measurements of profilometry was taken over the surface of each film, and results obtained shows an irregular surface as can be seen in that figure, results obtained shows depths with a minimum of 10µm and a maximum up to 150µm, but RMS analysis performed with this technique shows that surface tends to form a softer surface when the amount of tantalum is more in the growth process, this RMS factor was plotted and can be observed in **Figure 6**.

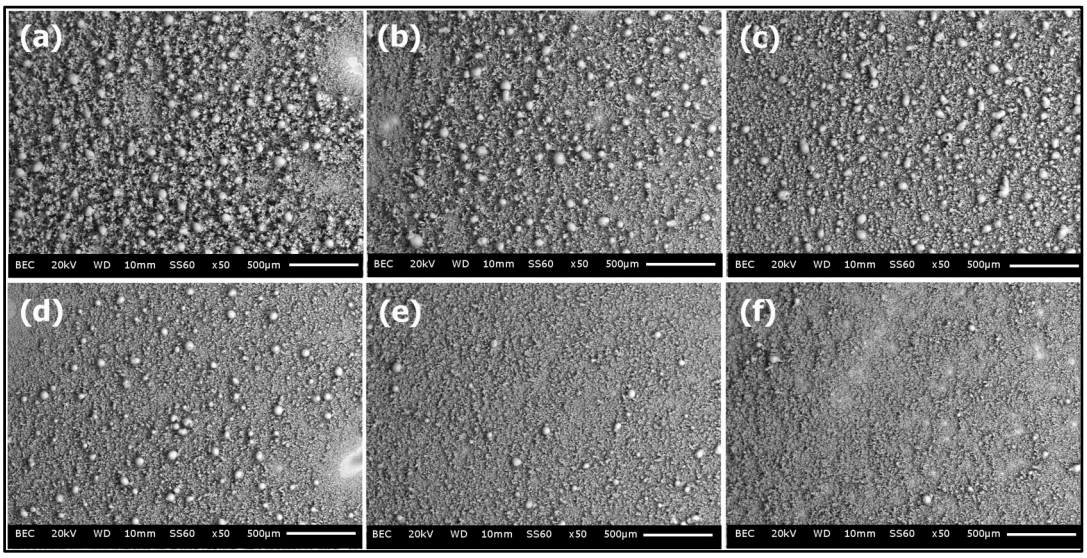

Figure 4.- Results SEM-50x of films ZnO:Ta doped growned on silicon substrates with (a) 0% Ta_2O_5, (b) 10% Ta_2O_5, (c) 20% Ta_2O_5, (d) 40% Ta_2O_5, (e) 50% Ta_2O_5, (f) 60% Ta_2O_5 on pill source.

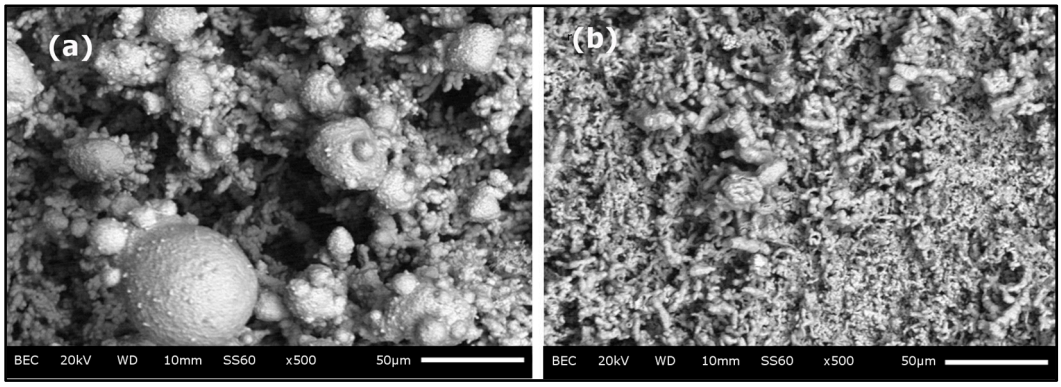

Figure 5. - Zoom 500x on film of (a) ZnO, and (b) ZnO:Ta doped with 60% on pill.

A detailed SEM image from those samples with a 500x zoom is shown in **Figure 5**. The surface is composed by spheres and rods in a random form like a porous sponge. Additionally, a FESEM analysis of **Figure 5**a and b displayed the same type of spherical structures but of different size. Some of those structures seem hollow or even broken showing a shell type structure, this shapes can be observed with a high resolution for ZnO in **Figure 7**a.1-a.3, and for ZnO:Ta doped in **Figure 7**b.1-b.3.

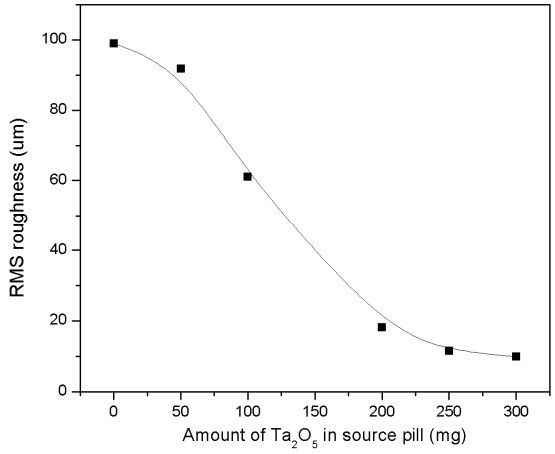

Figure 6. - Roughness dependence in films obtained according to amount of Ta in source pill.

Preprints (www.preprints.org) | NOT PEER-REVIEWED | Posted: 27 July 2018 doi:10.20944/preprints201807.0535.v1

Peer-reviewed version available at Crystals 2018, 8, 395; doi:10.3390/cryst8100395

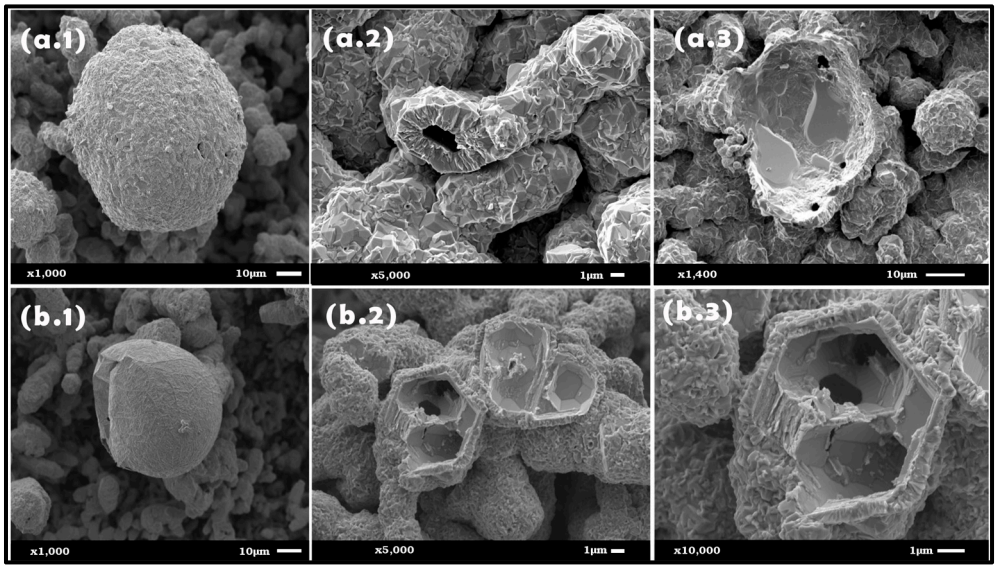

Figure 7. - High resolution SEM (FESEM) measurements for (a) undoped ZnO film, and (b) ZnO:Ta doped film in different zones of scanning.

From EDS analysis carried out on undoped ZnO films, oxygen and zinc elements were only detected (**Figure 8**a). The relation Zn/O greater than one indicate us the material is out of stoichiometry, which means a zinc rich ZnO material. Our results are in agreement with those found by other authors in this type of systems [21,36,37].

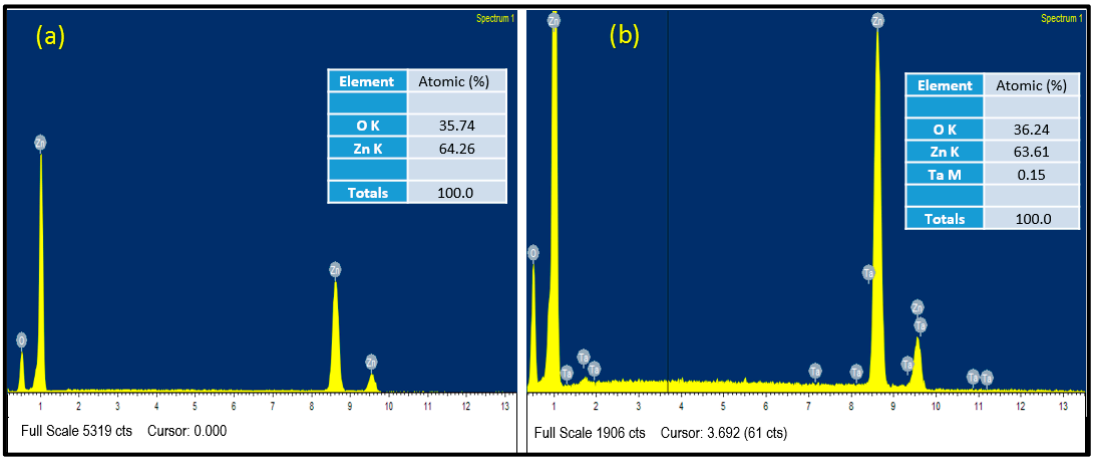

Figure 8. - EDS analysis for (a) undoped ZnO film, and (b) ZnO doped film with Ta atoms.

EDS results on Ta doped ZnO samples (**Figure 8**b) indicate us a Zn rich ZnO material but also a clear contribution of tantalum element around 0.1% and 0.15% in atomic percentage (±0.5% in weight), this could be owing to tantalum atoms are mainly incorporated inside the lattice of ZnO, but no over surface of the structures obtained.

The data above could give us light about the growth process. For undoped ZnO samples, the spheres could be formed as follow. Atomic hydrogen impact on the pill source producing OH^- (gas), Zn (gas) according to the reaction proposed in [21,23]. After that Zn atoms condensate in a vapor phase and some Zn liquid drops are formed and act as nucleation site and OH ions are attached to the surface forming a mixture of zinc in liquid state covered with a thin film of ZnO (solid) and they are deposited on the substrate where eventually coalesce and this drop increase in size. Further due to the presence of OH, the zinc oxide cover increases in thickness and a core(liquid)-shell(solid) structure is formed because of difference in the melting points 420°C and 1975°C for zinc and ZnO respectively.

As the growth is performed at high temperature, the nuclei remain in liquid state producing a Zn gas pressure due to vapor-liquid equilibrium and Zn atoms diffuses through the grain boundaries of the shell to release the internal pressure and eventually the shell is broken and Zn gas escape to the ambient producing holes on the shell as seen in **Figure 7**. This effect has been reported in the literature were hollow and concentric core-shell (Zn/ZnO) balls have been synthesized by oxidizing ZnO powders at low temperatures in air followed by an annealing at temperatures above the zinc melting point [23,38,39].

The existence of this crystalline zinc forming the core was detected by X-ray diffraction results (**Figure 1**) and by EDS where it was obtained a relation Zn/O of 69% at 31%, this means a zinc rich ZnO material.

On the other hand, for Ta doped ZnO samples, the way on the formation of this structures could be explained as a similar form as those undoped but instead of forming Zn liquid drops it forms a Zn-Ta alloy liquid drops. Because difference on the fusion point between Zn (420 °C) and Ta (2996 °C) the properties of the alloy changes and it can affect the size and form of the deposited material as seen in the sequence on **Figure 4**b-f. The more percentage of Ta_2O_5 the small structures are obtained. The shell is composed of small polyhedral crystals of ZnO material according to SEM, X-ray and Raman measurements.

Crystals forming the shell also are affected by the introduction of Ta as can be observed from FHSEM in **Figure 9**b. The ZnO composing the shell has like sheets polycrystalline shape with a smaller crystallite size than those undoped ZnO (see **Table 1**).

The effect of both decrease grain size and change in the shape of the crystals in ZnO:Ta doped films also have been observed and reported by different authors [24,40–43] and it is in agreement with our experiments. This effect could be owing to tantalum atoms creates a compression stress inside the lattice of ZnO and prevents an increase of this big shapes, this generated by the difference of ionic radii between Zn and Ta, as commented before in XRD results, in fact, this phenomenon also has been observed when ZnO is doped with tantalum by other techniques [40], or inclusive when ZnO is doped with other materials as aluminum and lithium [19,26].

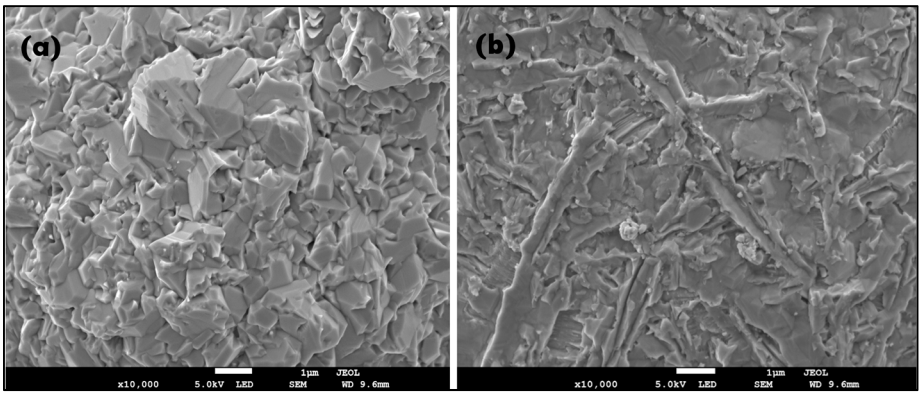

Figure 9.- FESEM measurements on shell from (a) undoped ZnO film, and (b) ZnO:Ta doped film

Synthesis of smaller structures means that somehow, that relation surface/volume of film increase, this fact will be reflected in an increment of reactions between existing species on the surface of structures, and also a possible increment in adsorption and resorption of species in this kind of porous films, and moreover and increment of cations or anions on the surface of film, as have been reported in other works, in fact, role of surface area has been observed to affect various mechanism as a gas sensors, biological cells, and effects of fluorescence emission [13,44–46].

3.4. Photoluminescence

Photoluminescence (PL) technique is a useful way to get information about energy states of impurities and defects of a material. **Figure 10** is shown the PL properties from our samples. As can be observed in that figure, all films exhibit two main bands, one sharp curve around of 380nm, and

another one more widened curve centered in 495nm and extended from 425nm to 625nm. The PL intensity first increases as the percentage of Ta increases, after that it decreases.

Photoluminescent emissions in ZnO have been grouped in two main bands denominated emissions near-band-edge (NBE) and deep levels emissions (DLE) corresponding to transitions band to band and transitions through to deep centers with energy levels in the forbidden gap respectively. Emissions NBE in ZnO have been attributed to the free excitons recombination and they are observed around the ultraviolet range.

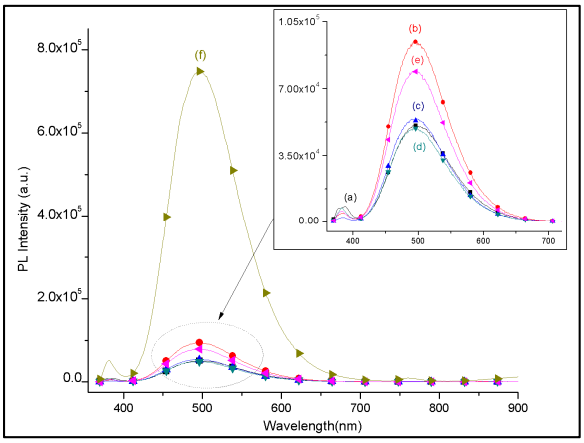

Figure 10.- Photoluminescence spectra of (a)ZnO film and ZnO:Ta doped films with (b) 10% Ta_2O_5, (c) 20% Ta_2O_5, (d) 40% Ta_2O_5, (e) 50% Ta_2O_5, (f) 60% Ta_2O_5 on pill source.

Nevertheless, emissions DLE in ZnO have been assigned to the presence of various point defects, either intrinsic or extrinsic that introduce deep levels in the bandgap and assumed as responsible of the PL band broadening in the range between blue and red emission [3,12,13,18,47].

As can be seen in **Figure 10**, the main PL band is the DLE band and it increases in intensity as the Ta_2O_5 is incorporated into the growth process by up to 60% and after that reduces. Moreover, all bands are peaked at the same wavelength independently of the percentage of Ta_2O_5 which means the contamination with Ta seems not to play a role in the generation of radiative deep centers other than those of uncontaminated ZnO.

To investigate the possible origin of the green luminescence observed in this type of films, a lot of reports that try to describe exactly this phenomena were reviewed, but actually there is no a consensus about this, because green emission has been observed on several films contaminated with Cu or Co atoms, on films with zinc vacancies (V_{Zn}), oxygen vacancies (V_O), interstitials zinc ions (Zn_i), oxygen antisites (O_{Zn}), and transitions Zn_i-->V_{Zn}, for this reasons, researchers came to the conclusion that this emission is a combination of several deep levels [47]. For example in reference [48], it was reported that when ZnO films were annealed at temperatures higher than 800℃, oxygen vacancies and zinc vacancies are generated, producing green emissions at 490 and 530nm. In addition, a good correlation between green emission and singly ionized oxygen vacancies was observed in commercial ZnO powders, annealed in forming gas (N_2 : H_2) or O_2 at temperatures ranging from 500 to 1050 ℃ [49].

By other side, has been reported that either, zinc vacancy and oxygen vacancy can contribute to green emission through of shallow donors, even Rodnyi and Khodyuk [47] reports that it is possible to assume the existence of donors with two levels (ground level and excited one) instead of two kinds of shallow donors. Also has been observed that in films of ZnO with an excess of oxygen, the maximum of green luminescence is around of 2.35eV and are zinc vacancies responsible of emission, but in ZnO films with an excess of zinc the maximum of luminescence is around of 2.53eV, and are oxygen vacancies acting as deep acceptor centers responsible for the observed emission.

In our case, the DLE emission observed is centered at 2.53 eV and according to with results presented above the films contain both zinc in excess and oxygen vacancies, therefore, those defects could be involved in the PL phenomena.

As can be observed in **Figure 10**, all DLE emissions obtained in these films are centered in 2.50eV (495nm), and except for curve f, all films present a broadening from 414nm to 630nm, as mentioned above, most intense peak can be attributed mainly to oxygen vacancies, and broadening of curve, can be assigned to a combination of different deep levels, either intrinsic or extrinsic.

Tantalum atoms introduce shallow donors in ZnO and modify its electrical conductivity but in this case, those centers seem no to play any effect on PL phenomena because zinc interstitials and oxygen vacancies are the defects involved in the PL phenomena.

Because the effect of the introduction of Ta atoms in ZnO is to increase the ratio volume surface as the structures area become smaller, the increase on the PL intensity could be attributed to a variation in the surface area of this films as has been shown in SEM section.

3.5. Hall mesuarements

It is well stablished ZnO has naturally type n conductivity because of the formation of intrinsic defects as oxygen vacancies and zinc interstitials during the synthesis. Oxygen vacancies can be easily formed and contribute with two free electrons to the conduction band. However, it has been shown that those defects are actually deep donors and cannot contribute to the n type conductivity. Therefore, zinc interstitials seem like the most probable defect acting as a donor in undoped ZnO films.

Carrier concentration, mobility, and resistivity of films measured by Hall-Vander Paw technique are presented in **Figure 11**. The majority carrier mobility first increases up to a maximum value and after reduces as the Ta_2O_5 percentage is increased in the growth while the carrier concentration increase as the Ta_2O_5 percentage does.

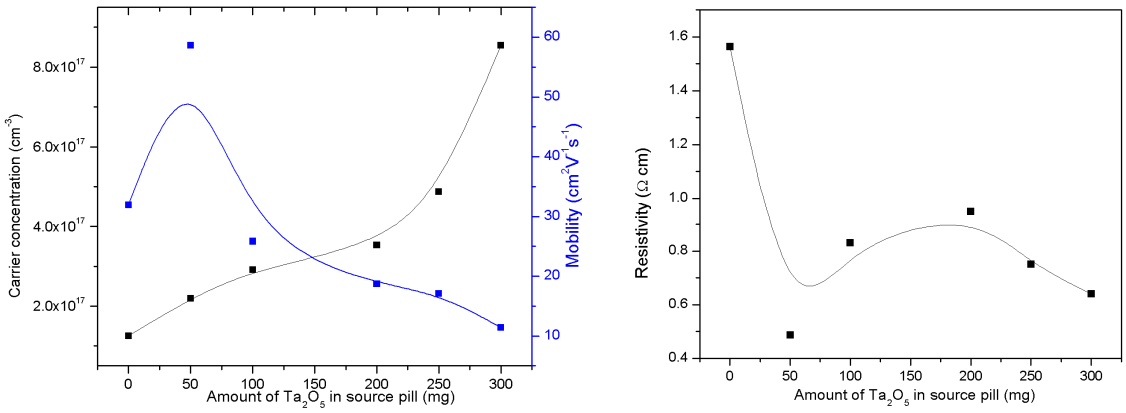

Figure 11. - Electrical characterization of ZnO and ZnO:Ta doped films: (a) carrier concentration and mobility, and (b) resistivity.

The minimum value of the carrier concentration is for undoped samples (**Figure 11**a) therefore, the increase of the concentration is for the incorporation of the Ta atoms in the Zn places of ZnO and they contribute with electrons to the conduction band. Carrier concentration is increasing as the amount of Ta_2O_5 is incremented in source pill, this could be a clear reason of increment in carrier concentration in ZnO:Ta doped films, since if a tantalum atom replace a zinc atom, this tantalum could have an oxidation state of Ta1+, Ta2+, or Ta3+ regarding to Zn, this means that tantalum is capable of contributing with free electrons.

The mobility (**Figure 11**a) initially increases with Ta_2O_5, reaching a maximum value in the film fabricated with 50mg of Ta_2O_5 in the source, after that, it starts to decrease. This effect has also been observed by K. Subha et al [42,43], and attributed to an excess of carriers in the ZnO lattice. Small increment observed in mobility is owing to a high number of free carriers generated by tantalum atoms, and the relative greater crystal size on the shell. Nevertheless, this mobility is reduced as the carrier concentration increases because this carrier creates a high number of collisions between them besides to the increase in the number of grain boundaries due to a reduction in the crystal size in the

shell. There are reports of ZnO with other dopants, in which it has been observed that foreign atoms inside the lattice of ZnO could act as charge trapping sites [17,26], which prevents the mobility of this free chargers. In our case, Ta atoms could be creating a similar effect, and therefore, mobility in our films decrease with the amount of Ta_2O_5 in the source pill.

Regarding to resistivity of the films, can be appreciated in **Figure 11**b that initially for ZnO film this has the highest value, but when these are doped with tantalum atoms, resistivity is around 0.5-1.0Ωcm, but this tends to decrease, this effect is attributed to excess of carriers generated by donors from Ta atoms incorporated in the ZnO lattice.

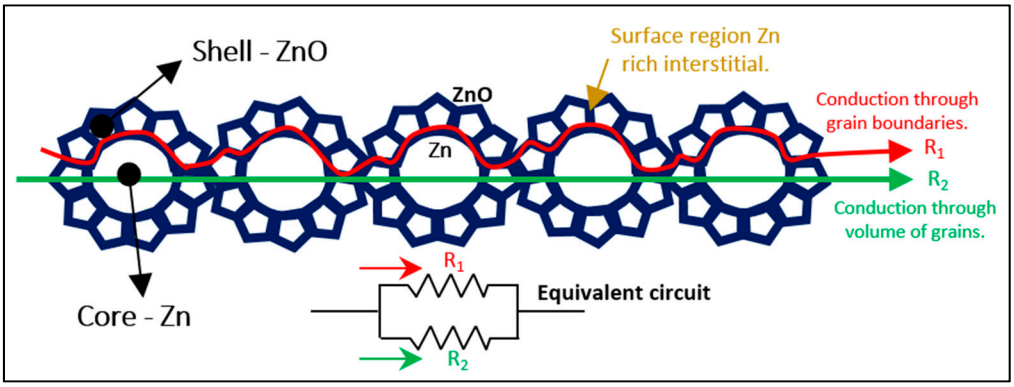

Figure 12. - Model of conductivity through crystal in the film. Two possible path for conduction: intergrain (R_1) and through volume of the grains (R_2).

To have a light about the conduction process in this type of films and an attempt to explain the results above the following a model is proposed in **Figure 12**.

First of all, we consider that the conduction of carriers in core shell structures could be a bit different from the pure crystals. As seen in SEM pictures (**Figure 7**), the core shell structures are composed by a metallic core and a shell formed by oxide crystals. Due to the high temperature of the process (above of the melting point of the zinc ~420 °C), zinc atoms diffuse through grain boundaries to release the internal pressure, creating zinc rich regions between grains. These zinc atoms became as suboxide with a higher concentration of zinc interstitials at the surface than in the grain volume. The effect creates a surface path for electric conduction while the grain volume with lower concentrations of interstitials has a low contribution to the conductivity.

When tantalum is introduced in the ZnO matrix, the concentration of carriers in the volume increases and the grain are capable of transport carriers, and resistivity of the film decreases as shown in **Figure 11**.

4. Conclusions

ZnO and ZnO:Ta doped films were obtained through of HFCVD approach, films have been obtained at 800°C in a hydrogen atmosphere, pill source was fabricated with a mixture powder of ZnO and Ta_2O_5. Films obtained were studied structural, morphological, compositional, optical and electrically, obtaining that, Ta atoms are incorporated into ZnO wurtzite structure but are not affecting this crystal lattice, owing to Ta atoms are substituting Zn atoms, and these are with similar atomic radii, nevertheless Ta atoms is benefiting growth direction (201) of ZnO, Raman spectroscopy confirm a majority contribution of ZnO in lattice, but Ta is not observed by this technique. According to EDS, films obtained, both ZnO and ZnO:Ta doped are Zn rich, but tantalum is presented in a low concentration, though tantalum is playing an important role in morphological structure, making that roughness decrease as the amount of Ta is increased in pill source, and by another hand, density of big sphere shapes tends to disappear, moreover, this technique confirms structures of kind core-shell. Photoluminescence studies reveals that films obtained are emitting in a range of green visible spectra, this effect mainly due to oxygen vacancies, tantalum atoms seems not to play an important role in creation of new centers of generation/recombination, but only in intensity of emission observed in 495nm, this owing to increment in surface area of the films. Electrical measurements expose that films

obtained are N-type, and tantalum atoms incorporated into the lattice of ZnO are contributing with a donor, increasing carrier concentration as Ta is increased in the film, also resistivity and the sheet resistance is decreasing when there is a greater amount of tantalum in the film.

Acknowledgments:

Authors gratefully acknowledge Dr. N. Rutilo Silva from IFUAP for FESEM images supported in this work, and Dr. M. Aceves from INAOE for PL measurements, as well as BUAP financial for support in publication fee, and CONACyT for Ph.D. support 304754 in the Institute of semiconductor devices program from BUAP.

References

1. Versteegh, M. A. M.; Vanmaekelbergh, D.; Dijkhuis, J. I. Room-Temperature Laser Emission of ZnO Nanowires Explained by Many-Body Theory. *Phys. Rev. Lett.* **2012**, *108*, 157402, doi:10.1103/PhysRevLett.108.157402.
2. Willander, M.; Nur, O.; Zhao, Q. X.; Yang, L. L.; Lorenz, M.; Cao, B. Q.; Ziga Pérez, J.; Czekalla, C.; Zimmermann, G.; Grundmann, M.; Bakin, A.; Behrends, A.; Al-Suleiman, M.; El-Shaer, A.; Che Mofor, A.; Postels, B.; Waag, A.; Boukos, N.; Travlos, A.; Kwack, H. S.; Guinard, J.; Le Si Dang, D. Zinc oxide nanorod based photonic devices: Recent progress in growth, lightemitting diodes and lasers. *Nanotechnology* **2009**, *20*, doi:10.1088/0957-4484/20/33/332001.
3. Willander, M.; Nur, O.; Sadaf, J. R.; Qadir, M. I.; Zaman, S.; Zainelabdin, A.; Bano, N.; Hussain, I. Luminescence from zinc oxide nanostructures and polymers and their hybrid devices. *Materials (Basel).* **2010**, *3*, 2643–2667, doi:10.3390/ma3042643.
4. Guo, L.; Zhang, H.; Zhao, D.; Li, B.; Zhang, Z.; Jiang, M.; Shen, D. High responsivity ZnO nanowires based UV detector fabricated by the dielectrophoresis method. *Sensors Actuators, B Chem.* **2012**, *166–167*, 12–16, doi:10.1016/j.snb.2011.08.049.
5. Könenkamp, R.; Nadarajah, A.; Word, R. C.; Meiss, J.; Engelhardt, R. ZnO nanowires for LED and field-emission displays. *J. Soc. Inf. Disp.* **2008**, *16*, 609, doi:10.1889/1.2918081.
6. Zheng, K.; Shen, H.; Li, J.; Sun, D.; Chen, G.; Hou, K.; Li, C.; Lei, W. The fabrication and properties of field emission display based on ZnO tetrapod-liked nanostructure. *Vacuum* **2008**, *83*, 261–264, doi:10.1016/j.vacuum.2008.07.010.
7. Seelig, E. W.; Tang, B.; Yamilov, A.; Cao, H.; Chang, R. P. H. Self-assembeled 3D photonic crystals from ZnO colloidal spheres. *Mater. Chem. Phys.* **2002**, *9712*, 1–7.
8. Pietruszka, R.; Witkowski, B. S.; Gieraltowska, S.; Caban, P.; Wachnicki, L.; Zielony, E.; Gwozdz, K.; Bieganski, P.; Placzek-Popko, E.; Godlewski, M. New efficient solar cell structures based on zinc oxide nanorods. *Sol. Energy Mater. Sol. Cells* **2015**, *143*, 99–104, doi:10.1016/j.solmat.2015.06.042.
9. Vittal, R.; Ho, K. C. Zinc oxide based dye-sensitized solar cells: A review. *Renew. Sustain. Energy Rev.* **2017**, *70*, 920–935, doi:10.1016/j.rser.2016.11.273.
10. Yazdi, M. A. P.; Martin, N.; Monsifrot, E.; Briois, P.; Billard, A. ZnO nano-tree active layer as heavy hydrocarbon sensor: From material synthesis to electrical and gas sensing properties. *Thin Solid Films* **2015**, *596*, 128–134, doi:10.1016/j.tsf.2015.08.065.
11. Chaudhary, S.; Umar, A.; Bhasin, K. K.; Baskoutas, S. Chemical sensing applications of ZnO nanomaterials. *Materials (Basel).* **2018**, *11*, 1–38, doi:10.3390/ma11020287.
12. Janotti, A.; Van De Walle, C. G. Native point defects in ZnO. *Phys. Rev. B - Condens. Matter Mater. Phys.* **2007**, *76*, doi:10.1103/PhysRevB.76.165202.
13. Jayakumar, O. D.; Sudarsan, V.; Sudakar, C.; Naik, R.; Vatsa, R. K.; Tyagi, A. K. Green emission from ZnO nanorods: Role of defects and morphology. *Scr. Mater.* **2010**, *62*, 662–665,

427 doi:10.1016/j.scriptamat.2010.01.020.
428 14. Gahlaut, U. P. S.; Kumar, V.; Pandey, R. K.; Goswami, Y. C. Highly luminescent ultra small Cu doped
429 ZnO nanostructures grown by ultrasonicated sol-gel route. *Optik (Stuttg).* **2016**, *127*, 4292–4295,
430 doi:10.1016/j.ijleo.2016.01.131.
431 15. Wang, Y.; Liu, N.; Chen, Y.; Yang, C.; Liu, W.; Su, J.; Li, L.; Gao, Y. Multicolour electroluminescence from
432 light emitting diode based on ZnO:Cu/p-GaN heterojunction at positive and reverse bias voltage. *RSC*
433 *Adv.* **2015**, *5*, 104386–104391, doi:10.1039/c5ra20569g.
434 16. Muthukumaran, S.; Gopalakrishnan, R. Structural, FTIR and photoluminescence studies of Cu doped
435 ZnO nanopowders by co-precipitation method. *Opt. Mater. (Amst).* **2012**, *34*, 1946–1953,
436 doi:10.1016/j.optmat.2012.06.004.
437 17. Klingshirn, C. ZnO: From basics towards applications. *Phys. Status Solidi Basic Res.* **2007**, *244*, 3027–3073,
438 doi:10.1002/pssb.200743072.
439 18. Özgür, Ü.; Alivov, Y. I.; Liu, C.; Teke, A.; Reshchikov, M. A.; Doğan, S.; Avrutin, V.; Cho, S. J.; Morko**,**
440 H. A comprehensive review of ZnO materials and devices. *J. Appl. Phys.* **2005**, *98*, 1–103,
441 doi:10.1063/1.1992666.
442 19. Chitra, M.; Uthayarani, K.; Rajasekaran, N.; Girija, E. K. Preparation and characterisation of Al doped
443 ZnO nanopowders. *Phys. Procedia* **2013**, *49*, 177–182, doi:10.1016/j.phpro.2013.10.024.
444 20. Liu, M.; Kitai, A. H.; Mascher, P. Point defects and luminescence centers in zinc oxide and zinc oxide
445 doped with manganese. *J. Lumin.* **1992**, *54*, 35.
446 21. López, R.; Díaz, T.; García, G.; Rosendo, E.; Galeazzi, R.; Coyopol, A.; Juárez, H.; Pacio, M.; Morales, F.;
447 Oliva, A. I. Fast formation of surface Oxidized Zn Nanorods and urchin-like microclusters. *Adv. Mater.*
448 *Sci. Eng.* **2014**, *2014*, doi:10.1155/2014/257494.
449 22. Richard, D.; Romero, M.; Faccio, R. Experimental and theoretical study on the structural, electrical and
450 optical properties of tantalum-doped ZnO nanoparticles prepared via sol-gel acetate route. *Ceram. Int.*
451 **2018**, *44*, 703–711, doi:10.1016/j.ceramint.2017.09.232.
452 23. Yuan, L.; Wang, C.; Cai, R.; Wang, Y.; Zhou, G. Temperature-dependent growth mechanism and
453 microstructure of ZnO nanostructures grown from the thermal oxidation of zinc. *J. Cryst. Growth* **2014**,
454 *390*, 101–108, doi:10.1016/j.jcrysgro.2013.12.036.
455 24. Cheng, Y.; Cao, L.; He, G.; Yao, G.; Song, X.; Sun, Z. Preparation, microstructure and photoelectrical
456 properties of Tantalum-doped zinc oxide transparent conducting films. *J. Alloys Compd.* **2014**, *608*, 85–
457 89, doi:10.1016/j.jallcom.2014.03.031.
458 25. Krishnan, R. R.; Vinodkumar, R.; Rajan, G.; Gopchandran, K. G.; Mahadevan Pillai, V. P. Structural,
459 optical, and morphological properties of laser ablated ZnO doped Ta2O5 films. *Mater. Sci. Eng. B Solid-*
460 *State Mater. Adv. Technol.* **2010**, *174*, 150–158, doi:10.1016/j.mseb.2010.03.065.
461 26. Bang, K.; Son, G. C.; Son, M.; Jun, J. H.; An, H.; Baik, K. H.; Myoung, J. M.; Ham, M. H. Effects of Li
462 doping on the structural and electrical properties of solution-processed ZnO films for high-performance
463 thin-film transistors. *J. Alloys Compd.* **2018**, *739*, 41–46, doi:10.1016/j.jallcom.2017.12.186.
464 27. Khan, A. Raman Spectroscopic Study of the ZnO Nanostructures. *J. Pakistan Mater. Soc.* **2010**, *4*, 5–9.
465 28. Schumm, M. ZnO-based semiconductors studied by Raman spectroscopy: semimagnetic alloying,
466 doping, and nanostructures, Doctoral dissertation, Julius–Maximilians University, 2008.
467 29. Soosen, S. M.; Koshy, J.; Chandran, A.; George, K. C. Optical phonon confinement in ZnO nanorods and
468 nanotubes. *Indian J. Pure Appl. Phys.* **2010**, *48*, 703–708.
469 30. Zhang, R.; Yin, P. G.; Wang, N.; Guo, L. Photoluminescence and Raman scattering of ZnO nanorods.

Solid State Sci. **2009**, *11*, 865–869, doi:10.1016/j.solidstatesciences.2008.10.016.

31. Tzolov, M.; Tzenov, N.; Dimova-Malinovska, D.; Kalitzova, M.; Pizzuto, C.; Vitali, G.; Zollo, G.; Ivanov, I. Vibrational properties and structure of undoped and Al-doped ZnO films deposited by RF magnetron sputtering. *Thin Solid Films* **2000**, *379*, 28–36, doi:10.1016/S0040-6090(00)01413-9.
32. Goff, A. H. Le; Joiret, S.; Saïdani, B.; Wiart, R. In-situ Raman spectroscopy applied to the study of the deposition and passivation of zinc in alkaline electrolytes. *J. Electroanal. Chem.* **1989**, *263*, 127–135, doi:10.1016/0022-0728(89)80129-9.
33. Marchebois, H.; Joiret, S.; Savall, C.; Bernard, J.; Touzain, S. Characterization of zinc-rich powder coatings by EIS and Raman spectroscopy. *Surf. Coatings Technol.* **2002**, *157*, 151–161, doi:10.1016/S0257-8972(02)00147-0.
34. Janotti, A.; Van De Walle, C. G. Fundamentals of zinc oxide as a semiconductor. *Reports Prog. Phys.* **2009**, *72*, doi:10.1088/0034-4885/72/12/126501.
35. Van De Walle, C. G.; Neugebauer, J. First-principles calculations for defects and impurities: Applications to III-nitrides. *J. Appl. Phys.* **2004**, *95*, 3851–3879, doi:10.1063/1.1682673.
36. López, R.; García, G.; Díaz, T.; Coyopol, A.; Rosendo, E.; Galeazzi, R.; Juárez, H.; Pacio, M. Low temperature growth of Zn-ZnO microspheres by atomic hydrogen assisted-HFCVD. *IOP Conf. Ser. Mater. Sci. Eng.* **2013**, *45*, 0–4, doi:10.1088/1757-899X/45/1/012016.
37. López, R.; Díaz, T.; García, G.; Galeazzi, R.; Rosendo, E.; Coyopol, A.; Pacio, M.; Juárez, H.; Oliva, A. I. Structural properties of Zn-ZnO core-shell microspheres grown by hot-filament CVD technique. *J. Nanomater.* **2012**, *2012*, doi:10.1155/2012/865321.
38. Lin, J. H.; Patil, R. A.; Devan, R. S.; Liu, Z. A.; Wang, Y. P.; Ho, C. H.; Liou, Y.; Ma, Y. R. Photoluminescence mechanisms of metallic Zn nanospheres, semiconducting ZnO nanoballoons, and metal-semiconductor Zn/ZnO nanospheres. *Sci. Rep.* **2014**, *4*, 1–8, doi:10.1038/srep06967.
39. Zhao, C. X.; Li, Y. F.; Zhou, J.; Li, L. Y.; Deng, S. Z.; Xu, N. S.; Chen, J. Large-scale synthesis of bicrystalline ZnO nanowire arrays by thermal oxidation of zinc film: Growth mechanism and high-performance field emission. *Cryst. Growth Des.* **2013**, *13*, 2897–2905, doi:10.1021/cg400318f.
40. Wu, Y.; Li, C.; Li, M.; Li, H.; Xu, S.; Wu, X.; Yang, B. Microstructural and optical properties of Ta-doped ZnO films prepared by radio frequency magnetron sputtering. *Ceram. Int.* **2016**, *42*, 10847–10853, doi:10.1016/j.ceramint.2016.03.214.
41. Krishnan, R. R.; Vinodkumar, R.; Rajan, G.; Gopchandran, K. G.; Mahadevan Pillai, V. P. Structural, optical, and morphological properties of laser ablated ZnO doped Ta2O5 films. *Mater. Sci. Eng. B Solid-State Mater. Adv. Technol.* **2010**, *174*, 150–158, doi:10.1016/j.mseb.2010.03.065.
42. Ravichandran, K.; Subha, K.; Dineshbabu, N.; Manivasaham, A. Enhancing the electrical parameters of ZnO films deposited using a low-cost chemical spray technique through Ta doping. *J. Alloys Compd.* **2016**, *656*, 332–338, doi:10.1016/j.jallcom.2015.09.115.
43. Subha, K.; Ravichandran, K.; Sriram, S. Combined influence of fluorine doping and vacuum annealing on the electrical properties of ZnO:Ta films. *Appl. Surf. Sci.* **2017**, *409*, 413–425, doi:10.1016/j.apsusc.2017.02.233.
44. Li, G.; Kawi, S. High-surface-area SnO ,: a novel semiconductor-oxide. *Mater. Lett.* **1998**, *34*, 99–102.
45. Bain, L. E.; Collazo, R.; Hsu, S. H.; Latham, N. P.; Manfra, M. J.; Ivanisevic, A. Surface topography and chemistry shape cellular behavior on wide band-gap semiconductors. *Acta Biomater.* **2014**, *10*, 2455–2462, doi:10.1016/j.actbio.2014.02.038.
46. Soni, U.; Sapra, S. The Importance of Surface in Core - Shell Semiconductor Nanocrystals. *J.Phys. Chem.*

2010, 22514–22518.

47. Rodnyi, P. A.; Khodyuk, I. V. Optical and luminescence properties of zinc oxide (Review). *Opt. Spectrosc.* **2011**, *111*, 776–785, doi:10.1134/S0030400X11120216.

48. Studenikin, S. A.; Golego, N.; Cocivera, M. Fabrication of green and orange photoluminescent, undoped ZnO films using spray pyrolysis. *J. Appl. Phys.* **1998**, *84*, 2287–2294, doi:10.1063/1.368295.

49. Vanheusden, K.; Warren, W. L.; Seager, C. H.; Tallant, D. R.; Voigt, J. A.; Gnade, B. E. Mechanisms behind green photoluminescence in ZnO phosphor powders. *J. Appl. Phys.* **1996**, *79*, 7983–7990, doi:10.1063/1.362349.